

Testing Dark Energy models vs Λ CDM Cosmology by Supernovae and Gamma Ray Bursts

L. Izzo^{1,2,3}, S. Capozziello¹, G. Covone¹ and M. Capaccioli^{1,4}

¹ Dipartimento di Scienze Fisiche, Università di Napoli "Federico II" and INFN Sez. di Napoli, Compl. Univ. Monte S. Angelo, Ed. N, Via Cinthia, I-80126 Napoli, Italy,

² ICRA and ICRA, Piazzale della Repubblica 10, I-65122 Pescara, Italy,

³ Dip. di Fisica, Università di Roma "La Sapienza", Piazzale Aldo Moro 5, I-00185 Roma, Italy,

⁴ INAF - VSTceN, Salita Moiarillo, 16, I-80131, Napoli, Italy

Preprint online version: July 12, 2021

ABSTRACT

Aims. A new method to constrain the cosmological equation of state is proposed by using combined samples of gamma-ray bursts (GRBs) and supernovae (SNeIa).

Methods. The Chevallier-Polarski-Linder parameterization is adopted for the equation of state in order to find out a realistic approach to achieve the deceleration/acceleration transition phase of dark energy models.

Results. As results, we find that GRBs, calibrated by SNeIa, could be, at least, good distance indicators capable of discriminating cosmological models with respect to Λ CDM at high redshift. Besides, GRBs+SNeIa combined redshift-distance diagram puts better in evidence the change of slope around redshift $z \sim 0.5$ which is usually addressed as the "signature" of today observed acceleration. This feature could be interpreted, in more standard way, by the red sequence in galaxy clusters.

Key words. Gamma rays : bursts - Cosmology : cosmological parameters - Cosmology : distance scale

1. Introduction

From an observational viewpoint, one of the fundamental question of cosmology is measuring cosmological distances and then to build up a suitable and reliable cosmic distance ladder. This issue has recently become even more important due to the evident degeneracy of several dark energy models with Λ CDM, despite the advent of the so-called Precision cosmology, (Ellis 1999).

More precisely, in the last two decades, a class of accurate standard candles, the Supernovae Ia (SNeIa) has been highly studied and the results obtained from the use of these objects led to the surprising discovery of the apparent acceleration of the cosmic Hubble flow (for a review see (Kowalski et al 2008)). However these objects are hardly detectable at redshifts higher than ~ 1.5 , so we need distance indicators at higher redshifts in order to remove the disturbing degeneration of dark energy models today affecting the current cosmological picture (Λ CDM is a good approximation of the observed Universe, also if there is yet no theoretical basis about the nature of its components, but the issue of global evolution is far from being addressed, for a comprehensive review see (Copeland et al 2006)). A possible way out for this problem could be found by adopting Gamma Ray Bursts (GRBs) as distance indicators also if it is premature, at the moment, to speak about standard candles.

As it is well known, GRBs are the most powerful explosions in the Universe: the most likely scenarios for their generation are the formation of massive black holes or the coalescence of binary stellar systems. These events are observed at considerable distances, so there are several efforts to frame them into the standard of cosmological distance ladder. In literature, there are several models that give account for the GRB formation. The standard model (Meszaros 2006) predicts the formation of a black

hole originated by a massive star whose core is going to collapse. Alternatively, the GRB phenomenon could be generated during an accretion episode followed by a merging event which gives rise to a jet-like outflow. For the class of short GRBs (which time duration is less than 2 seconds), the candidates are mergers of neutron stars. Another model, (Ruffini et al 2008), includes different central energy sources and the formation of charged black holes.

All these scenarios retain essentially a similar shock phenomenon: a "fireball" or a "fireshell". Here we will not go into details, but it is worth stressing that none of these models is intrinsically capable of connecting all the observable quantities.

Despite of the poor knowledge of the GRB mechanism, it seems that GRBs could be used as reliable distance indicators. In fact there exist several observational correlations among the photometric and spectral properties of GRBs which point out that it could be realistic to suppose them as distance indicators, (Basilakos & Perivolaropoulos 2008; Ghirlanda et al 2006). Nevertheless the origin of these spectroscopic and photometrical correlations is not known very well and there are several efforts to interpret the behavior of GRB features in a coherent way, by relatively simple scenarios (e.g. see (Dainotti et al 2008; Ghisellini et al 2008)). Succeeding in explain the mechanism that generates the GRBs is one of the objectives of the modern astrophysics and to clarify these observed correlations in this context would make GRBs as reliable distance indicators. A complete review of the existing luminosity relations for GRBs can be found in (Schaefer 2007).

In this paper, we consider two relations, the one by Liang-Zhang (LZ), (Liang & Zhang 2005), and the one by Ghirlanda (GGL), (Ghirlanda et al 2004). They are the only 3-parameters relations and have less scatter with respect to the theoretical

best fit than the other 2-parameters ones. In a recent paper, (Capozziello & Izzo 2008), starting from a sample of GRBs, a GRB-Hubble diagram has been derived considering these relations. However it is worth noticing that the calibration of the used relations has been necessary in order to avoid the circularity problem. This means that all the relations need to be calibrated for every set of cosmological parameters. Indeed, all GRB distances, obtained in a photometric way, are strictly dependent on the cosmological parameters since, currently, there is no low-redshift (z up to 0.2-0.3) set of GRBs to achieve a cosmology-independent calibration. In order to overcome this difficulty, Liang et al., (Liang et al 2008), proposed a method in which several GRB-relations have been calibrated by SNeIa. In fact, supposing that our relations work at every redshift and that, at the same redshift, GRBs and SNeIa have the same luminosity distance, it becomes possible, in principle, to calibrate the GRB-relations using an interpolation algorithm. In this way, it becomes possible building a GRB-Hubble diagram by calculating the luminosity distance for each GRB with the well-known relation between the luminosity distance d_l and the energy-flux ratio of the distance indicators, i.e.

$$d_l = \left(\frac{E_{iso}}{4\pi S'_{bolo}} \right)^{\frac{1}{2}}, \quad (1)$$

where E_{iso} is the isotropic energy emitted in the burst and S'_{bolo} is the bolometric fluence corrected to the rest frame of the source in consideration. This result can be connected to the Hubble series, (Visser 2004), and the density parameters Ω_M and Ω_Λ can be obtained. The results in (Capozziello & Izzo 2008) were in agreement with the other observations but the estimation of the CPL-parameters (Chevallier et al 2001), which is an advantageous parameterization of cosmological Equation of State (EoS) $w = p/\rho$, (see for a brief review of the various parameterizations of the EoS the work by (Barboza & Alcaniz 2008)), is only marginally consistent with the data existing in the literature, (e.g. see the already cited work by Visser). The reason of this disagreement is due to the fact that the method used in (Capozziello & Izzo 2008) works very well at redshift less than $z \simeq 1$ while CPL parameters are supposed to work also at high redshift.

The aim of this paper is to take into account a cosmological EoS working at any redshift, using GRBs as tracers and adopting again the CPL parameterization. The layout of the paper is the following: in Sect. 2, we discuss the method which, in principle, should allow to obtain a cosmology-independent formulation of the luminosity distance and then of the distance modulus. Sect. 3 is devoted to a discussion of the GRB luminosity-relations considered in this work. In Sect. 4, we illustrate the fitting of the data obtained by these relations while results and perspectives of the approach are discussed in Sect. 5.

2. The cosmological model

The goal is to obtain an analytic formulation of the Hubble diagram valid, in principle, at any redshift. Let us start from the Friedmann equation

$$H^2 = \frac{8\pi G}{3}\rho - \frac{kc^2}{a^2}. \quad (2)$$

We obtain, by some algebra, the following equation in terms of the density parameter

$$H^2 = H_0^2 \left[\Omega_0 \left(\frac{a_0}{a} \right)^{3(w+1)} - (\Omega_0 - 1) \left(\frac{a_0}{a} \right)^2 \right], \quad (3)$$

where the subscript 0 indicates the present value of the parameters. From now onwards, we take into account a spatially quasi-flat Universe, $k \approx 0$, the contribution of the curvature will be negligible and we have $\Omega_0 \approx 1$, as suggested by the latest CMBR (Komatsu et al 2008) and the SNeIa observations (Kowalski et al 2008). However in the final section, we will do a test to verify this assumption with observations coming from GRBs. Now if we translate in terms of redshift z ,

$$\frac{a_0}{a} = 1 + z, \quad (4)$$

the previous equation reduces to

$$H^2(z) = H_0^2 (1 + z)^{3(w+1)}. \quad (5)$$

The w -parameter indicates the EoS $w = p/\rho$, where p and ρ are the pressure and the matter-energy density of the Universe, respectively. Considering the CPL parameterization of the EoS, (Chevallier et al 2001):

$$w(z) = w_0 + w_a \frac{z}{1+z}, \quad (6)$$

and substituting into Eq.(5), we obtain:

$$H(z) = H_0 \left[(1 + z)^{\frac{3}{2}(w_0 + w_a + 1)} \exp \left(\frac{-3w_a z}{2(1+z)} \right) \right], \quad (7)$$

which enters directly in the expression of the distance modulus

$$\mu(z) = -5 + 5 \log d_l(z), \quad (8)$$

where $d_l(z) = c(1+z)D_l(z)$ and where

$$D_l(z) = \int_0^z \frac{d\xi}{H(\xi)}. \quad (9)$$

This means that an analytic expression for μ can be achieved. The integral D_l in Eq.(9) can be solved giving a Gamma function of the first kind¹:

$$D_l(z) = \left(\frac{3w_a}{2} \right)^{-\frac{1+3w_0+3w_a}{2}} \exp \left(\frac{3w_a}{2} \right) \Gamma \left[\frac{1+3w_0+3w_a}{2}, \frac{3w_a}{2(1+\xi)} \right]_{\xi=0}^{\xi=z}. \quad (10)$$

Substituting such an expression in the distance modulus, we obtain a model for data fitting which could work, in principle, at any z . It is important to stress that the obtained expression for the Hubble parameter $H(z)$ is independent of the density parameters, Ω_M and Ω_Λ , provided that their sum is equal to 1.

It is worth noticing that we are using the CPL parameterization not only for the dark energy component, but for the total energy-matter density of the Universe. This assumption works because dark and baryonic matter are contributing with a null pressure while the radiation component is negligible in matter- and dark energy-dominated eras. Furthermore, the analytical formulation which we are adopting for the luminosity distance is assumed valid at any redshift z .

¹ In our case, the variable of the Gamma function, z , is always positive so that we have no problem of discontinuity in applying the Gamma function in the following calculations.

3. GRBs luminosity relations

As we said, GRBs are the most powerful explosions in the Universe, so they can be observed up to very far distances. Theoretically, they can be observed up to a redshift of the order $z \sim 10$. Some considerations on the spectrum of such sources are due at this point. The electromagnetic emission spectrum of GRBs ranges from radio up to gamma wavelengths, but the main bulk of emission is in the gamma band. In the last years, thanks to several spacecraft missions capable of observing this high energy region, the main features of GRBs have been better known. Recently, some photometric and spectroscopic relations between GRB observables have been found and then the hypothesis that these objects could be considered suitable distance indicators has been seriously considered. Nevertheless, up to now, there is no theoretical model that fully explains these relations so the GRBs cannot be considered as standard candles in a proper sense. For a detailed review of the observational features see (Schaefer 2007).

Here, we are taking into account the existing 3-parameter relations. This choice has been done because these relations put the better constraints on the data giving less scatter between the theoretical relation and the experimental data (e.g. see (Schaefer 2007)). The first relation is the so-called Liang-Zhang relation, (Liang & Zhang 2005), which allows to connect the GRB peak energy, E_p , with the isotropic energy released in the burst, E_{iso} , and with the jet break - time of the afterglow optical light curve in the rest frame, measured in days, t_b , that is

$$\log E_{iso} = a + b_1 \log \frac{E_p(1+z)}{300keV} + b_2 \log \frac{t_b}{(1+z)1day} \quad (11)$$

where a and b_i , with $i = 1, 2$, are calibration constants.

The other one is the relation given by Ghirlanda et al. (Ghirlanda et al 2004). It connects the peak energy E_p with the collimation-corrected energy, or the energy release of a GRB jet, E_γ , where

$$E_\gamma = F_{beam} E_{iso}. \quad (12)$$

and $F_{beam} = 1 - \cos \theta$, with θ_{jet} the jet opening angle defined in (Sari et al. 1999):

$$\theta_{jet} = 0.163 \left(\frac{t_b}{1+z} \right)^{3/8} \left(\frac{n_0 \eta_\gamma}{E_{iso,52}} \right)^{1/8}, \quad (13)$$

where $E_{iso,52} = E_{iso}/10^{52}$ ergs, n_0 is the circumburst particle density in 1 cm^{-3} , and η_γ the radiative efficiency. The Ghirlanda et al. relation is

$$\log E_\gamma = a + b \log \frac{E_p}{300keV}, \quad (14)$$

where a and b are two calibration constants.

From these relations, we can obtain directly the luminosity distance d_l from the well-known formula which connects d_l with the isotropic energy E_{iso} and the bolometric fluence S_{bolo} :

$$d_l = \left(\frac{E_{iso}}{4\pi S_{bolo}} \right)^{1/2}, \quad (15)$$

from which it is easy to compute, for each GRB, the distance modulus μ and its error given by (Liang et al 2008):

$$\sigma_\mu = \left[(2.5\sigma_{\log E_{iso}})^2 + (1.086\sigma_{S_{bolo}}/S_{bolo})^2 \right]^{1/2} \quad (16)$$

Table 1. Results of the fits. SNeIa is only for the Supernova Ia data, LZ is for the GRBs data obtained from the Liang-Zhang relation, GGL for the Ghirlanda et al. one. Note the improvement on the w -parameter using the GRBs data in addition to the SNeIa data corrected for the 3 “outlier” GRBs.

Relation	w_0	w_a	R^2
SNeIa	-0.910 ± 0.070	0.755 ± 0.054	0.983
LZ	-1.39 ± 0.38	1.18 ± 0.37	0.817
GGL	-1.46 ± 0.38	1.36 ± 0.32	0.812
LZ + SNeIa	-1.15 ± 0.10	0.93 ± 0.11	0.933
GGL + SNeIa	-1.42 ± 0.12	1.24 ± 0.13	0.920

with $\sigma_{\log E_{iso}}$ and $\sigma_{S_{bolo}}$ obtained from the error propagation applied to Eq.(11) and Eq.(14). Moreover, we assume that the error in the determination of the redshift z is negligible, as well as for the radiative efficiency η_γ . We note also that the assumption of a well-known n_0 is a strong hypothesis since the goodness of the fits depends, in particular, on this parameter. However, we are going to consider the n_0 values for each GRB given in the Table 5 also if it lacks a complete and clear physical basis for the considered relations, (Friedman & Bloom 2005). The GRB data sample is taken from the already cited work by Schaefer. We take into account 27 events with extremely precise data. Such a sample is the same adopted in (Capozziello & Izzo 2008).

4. The data fitting

The next step is the fit of the GRB sample with the empirical relations, Eqs.(11),(14), described in Sect. 3. The aim is to achieve an estimate of the CPL parameters and consequently to determine the trend of the EoS at any redshift, using the analytical relation, Eq.(10). As we said, we are considering the same sample of 27 GRBs used in (Capozziello & Izzo 2008), see Table 5, in which we have added the sample of SNeIa by the Union Supernova Survey, (Kowalski et al 2008).

The numerical results of the fits are shown in Table 1, where we obtain a robust estimation of the CPL parameters for both the relations used, with and without SNeIa data. An immediate comparison is done with the best fit applied only to the SNeIa sample. It is evident how adding GRBs to SNeIa data improves the knowledge and the precision on the EoS parameter w . In Fig. 1, the best fit curve, in the case of LZ relation, is plotted while, in Fig. 2, it is plotted the best fit curve for the SNeIa data using the theoretical model described previously.

In order to measure the goodness of the fit, we use the R^2 test for an accurate reliability, see Table 1. The R^2 test is a measure of how successful the fit is in explaining the variation of the data (see for details (Draper & Smith 1998)). Exactly an R^2 close to 1.0 indicates that we have accounted for almost all of the variability with the data specified in the model. As standard, the R^2 test is the square of the correlation between the response values and the predicted response values, that is:

$$R^2 = 1 - \frac{SSE}{SST} = 1 - \frac{\sum_{i=1}^n w_i (y_i - \hat{y}_i)}{\sum_{i=1}^n w_i (y_i - \bar{y}_i)^2}, \quad (17)$$

where SSE is the sum of the squares due to errors and it measures the total deviation of the response values from the fit and SST is the sum of squares about the mean: \hat{y} is the predicted response value, \bar{y} is the mean value and the w_i are the weights on the values.

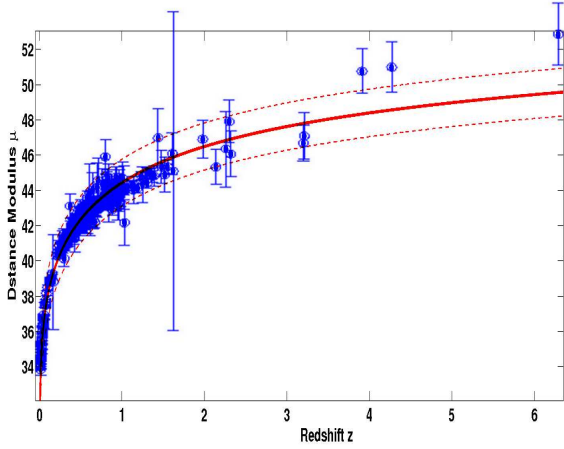


Fig. 1. Redshift-Distance modulus diagram for the GRB+SNeIa sample. The black dots are the GRBs, the blue ones are the SNeIa. The red line is the best fit obtained from the data, with the dashed line representing the confidence limits at 3σ . The error bars on the Supernova data are not represented because they are negligible.

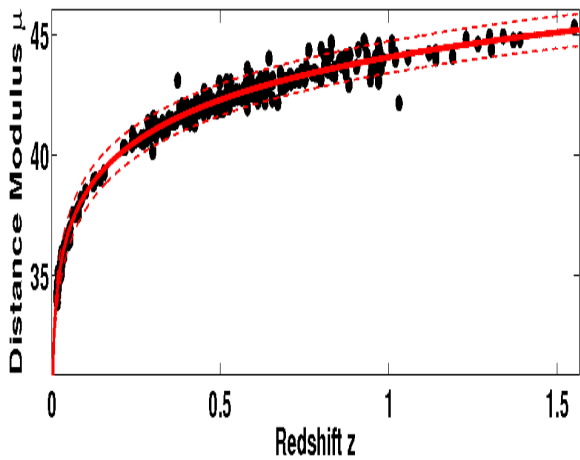


Fig. 2. Redshift-Distance modulus diagram for the SNeIa sample only. The black dots are the Supernova data while the red line is the best fit obtained from the data. The error bars on the Supernova data are not represented because they are negligible.

A further consistency test for the adopted samples of GRBs and SNeIa can be derived considering the relation $(\log d_l)^{1/4} - \text{redshift}$ vs z . In such a way, data from GRBs and SNeIa can be better separated in order to track the whole trend of both sets and showing, in particular, the spreading of GRB distribution. In Fig. 3, the results of this relation is plotted and it is reasonable to conclude that SNeIa could be used to calibrate GRBs at lower redshifts. In particular, it is evident, even considering the only SNeIa data, a change in the trend at redshift included between $z = 0.3$ and $z = 0.5$.

In particular, the extension of the Supernova Hubble Diagram with the GRB data can be used to improve our knowledge of the trend at high redshift. In this way, using also the GRB data, we build a plot, Fig. 5, where the distance modulus μ versus the redshift z , in a logarithmic scale, is plotted. The best fit curve, obtained with the method described previously, Eq.(10), is also reported. However in order to better point out this varia-

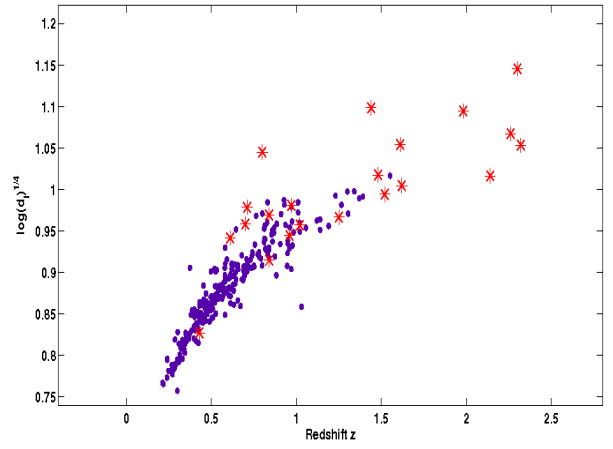


Fig. 3. Comparison between GRBs-SNeIa data using the relation $(\log d_l)^{1/4}$ for each data sample. Blue dots are the SNeIa while the red star are the GRBs. We are considering redshifts between 0 and 3, in order to better analyze the data trend in the overlapping redshift range.

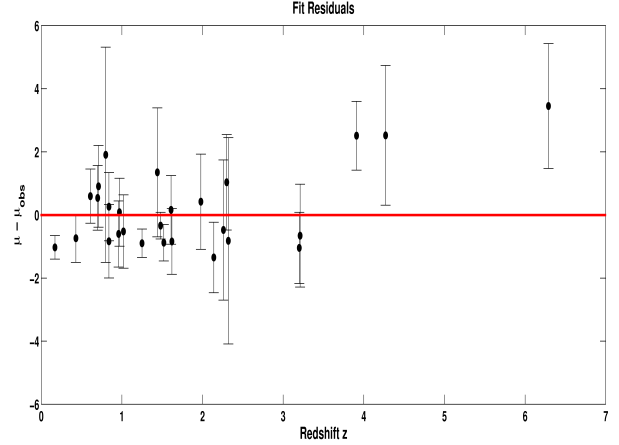


Fig. 4. Comparison between the best fit of μ and the observed distance modulus μ_{obs} at any redshift. The black dots are the GRBs data and the red line is the best fit curve representing the theoretical distance modulus.

tion, we have done an extended analysis, Fig. 6, where we considered the GRB+Snn sample up to a certain value of the redshift z_t and its complementary, and then we fitted these samples with a simple curve of the type $a_i + b_i \log z$, with the cut-redshift z_t ranging from $z_t = 0.1$ to $z_t = 0.6$ with redshift-step 0.1. The result of this analysis is given in Table 2, where we note that at redshift greater than $z_t = 0.5$, the two best fit curves tend slowly to coincide, suggesting that something happens at redshift smaller than this value. This result led in the past to the conclusion that the universe is accelerating.

It is suggestive to link the observed behaviour of the cosmological acceleration to the the formation and evolution of astrophysical structures. For instance, the infalling rate of field galaxies (Stott et al. 2009) could be related to the overall expansion rate.

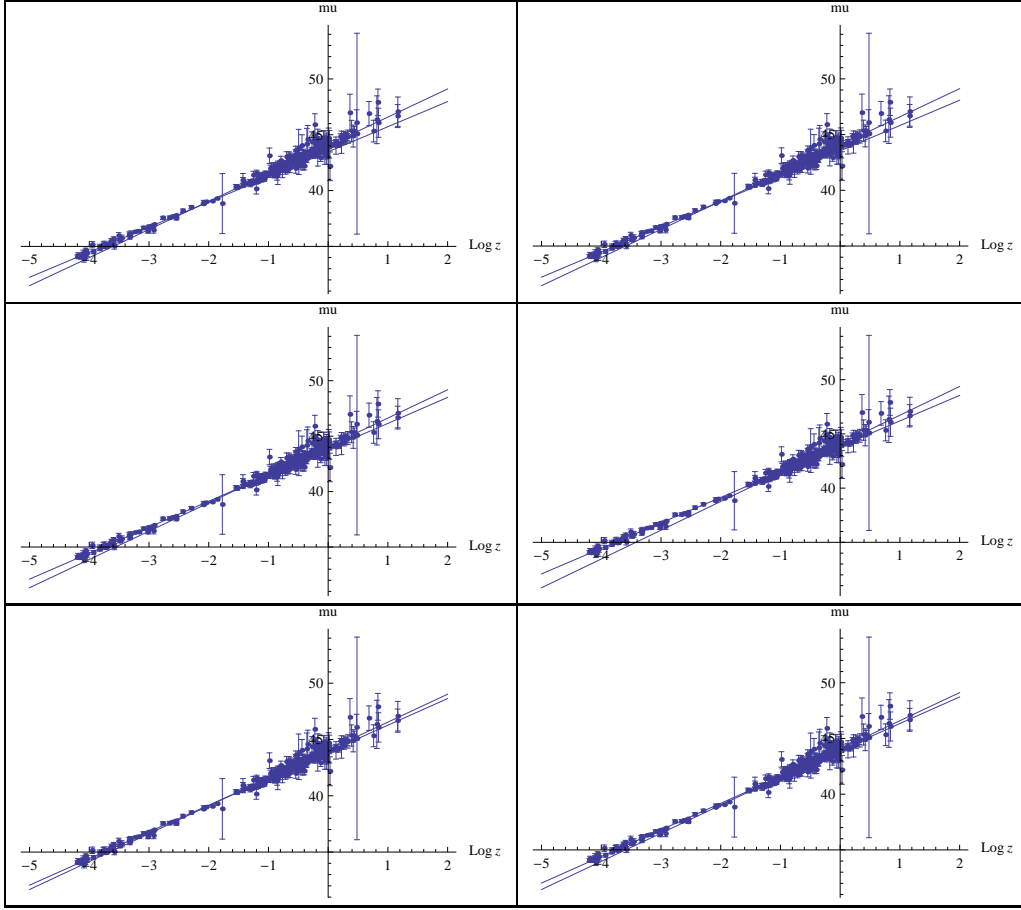


Fig. 6. Redshift-Distance modulus diagram for the GRB+SNeIa samples versus $\log z$ as described in the text. Note the “linearization” of the two best fit curves of the two data samples, done with the model $a_i + b_i \log z$, obtained considering only GRB and Sn data up to and beyond, respectively, the cut-redshift value z_t , with z_t ranging from $z_{tmin} = 0.1$ and $z_{tmax} = 0.6$ with step of $z_{step} = 0.1$.

Table 2. Results of the logarithmic fit described in the text and plotted in fig. 6

z_t	a_1	b_1	a_2	b_2
0.1	44.07	2.52	43.48	2.25
0.2	44.07	2.52	43.55	2.28
0.3	44.08	2.55	43.81	2.34
0.4	44.07	2.65	43.85	2.35
0.5	44.06	2.48	43.90	2.37
0.6	44.06	2.52	43.95	2.38

It would be very interesting to assess quantitatively such a relation, from the massive galaxy clusters with some good indicator at that redshift in order to clarify a possible correlation between these two phenomena. All of these cosmological and astrophysical hints lead us to reconsider from a different point of view the possible cause of the apparent acceleration of the Universe which could be addressed to some more astrophysical standard effects, (Izzo et al. in preparation).

In Fig. 4, it is plotted the comparison between the theoretical μ_{th} and the observed distance modulus μ_{obs} at any redshift, the residual plot. A smooth trend up to $z \approx 3.5$ in the residual curve can be immediately detected. Beyond this limit, we have 3 GRBs that exceed, by the same side, the 3σ confidence limit of the best fit. This discrepancy is clear in Fig. 5, where is plotted the best fit for the combined sample in the case of LZ relation with a logarithmic scale for the redshift. It is worth noticing that a similar, but opposite discrepancy was obtained by

(Perivolaropoulos & Shafieloo 2008) using only the SNeIa sample. In that paper, the authors found a brightening for the SNeIa at high redshift, while here, we find a sort of “darkening” for the GRBs at redshift higher than $z = 4$.

This fact is fundamental for the goodness of the fit because these GRBs represent the most distant objects that one can use to make such an analysis and their weight on the fit is very high, in the sense that they appear to be not accurate distance indicators. There could be several explanation for this anomalous GRB brightness at high redshift and the most likely are the following:

- there is some process of absorption of gamma radiation where the GRB γ photons may interact with the very low energy photons incoming from the cosmic thermal background radiation, (Zdziarski and Svensson 1989);
- these 3 GRBs could be outliers;

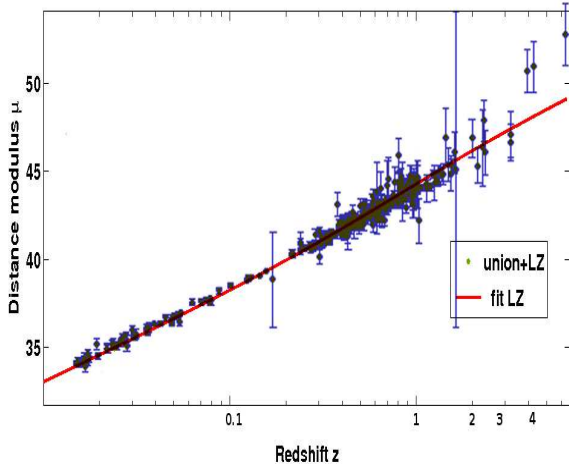


Fig. 5. Redshift-Distance modulus diagram for the GRB+SNeIa sample versus redshift in logarithmic scale.

- the Circum Burst Density (CBD) in the host galaxy at that epoch, $z > 4$, could be different from the CBD in galaxies at low redshift;
- there could be some high-energy bias: since at that distances only very powerful GRBs can be observed, some high-energy process, involving very energetic γ -photons, (Kelner et al. 2008; Razzaque et al. 2009), could happen so that the flux received by our detectors is dimmed;
- it could be that the CPL parameterization, or the Λ CDM model, is a bad approximation for the cosmological EoS.

It is very interesting to note that this phenomenon is very similar to the change in the trend of the Supernovae Ia data, as we mentioned earlier. However, at these redshifts is very difficult to make any kind of astrophysical constraint, since there is not enough information about this region of the Universe.

Nevertheless, we repeat the analysis described above without these 3 GRBs obtaining a better value than the previous one for the R^2 test. The results of these corrected fits are shown in the table 4. In Fig. 7, it is plotted the best fit with this corrected sample. From these results we conclude that the complete sample gives different results from the corrected sample, the first one suggesting a phantom/quintessence regime for the present epoch while the second one can be enclosed in the case of an accelerating Λ CDM model. This last result is confirmed by the following analysis, where we have performed a Monte-Carlo-like procedure for the comparison of the results with the usual likelihood estimator given by

$$\chi^2 = \sum_{i=1}^N \left[\frac{(\mu_{th}(z_i) - \mu_{obs}(z_i))^2}{\sigma_i} \right], \quad (18)$$

in the context of a Λ CDM model of the Universe, where μ_{th} is the distance modulus computed from the Eq.(8) and Eq.(9), z_i is the observed redshift for each GRB and σ_i the observed distance modulus uncertainty. The results of this analysis are shown in the Table 3, where we can see the improvement obtained by the GRB sample corrected for the 3 "wrong" GRBs. In Fig.(8), it is shown the contour plot of the corrected sample, where the boundaries correspond to 1σ , 2σ and 3σ confidence levels. In this, case we do not consider a purely flat geometry, as we previously said in the Sect. 2, but we constraint the k -parameter of Eq.(2) to vary between the value $-0.05 < k < 0.05$ so that we take account of a possible small contribution due to the curvature density.

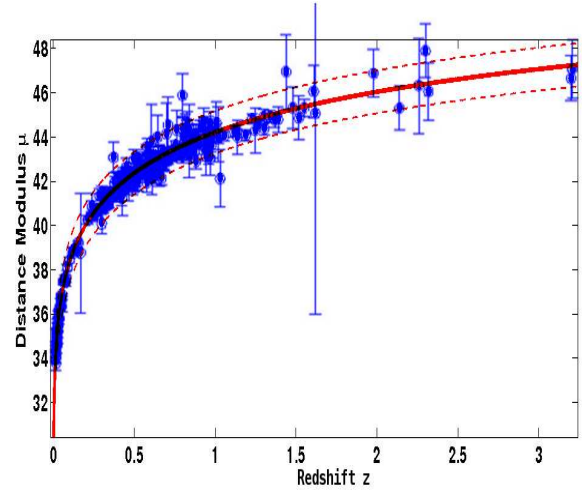


Fig. 7. Redshift-Distance modulus diagram for the corrected GRB+SNeIa sample. The red line is the best fit obtained from the data, with the dashed line representing the confidence bounding at 3σ .

We have adopted a similar procedure in the case of an EoS evolving with redshift and where μ_{th} is obtained by the Eq.(10). The result of this analysis is plotted in Fig. 9 where the best fit value, the cross in the figure, corresponds to the value $w_0 = -0.84 \pm 0.14$ and $w_a = 0.72 \pm 0.06$, in a good agreement with the results obtained, see Table 4, using our theoretical relation, Eq.(10).

Summarizing, from this analysis, we conclude that the corrected sample agrees fairly well with the Λ CDM model with a small contribution of the curvature parameter, being equal to $k = 0.01 \pm 0.04$. In other words, the method delineated in the Sect.2 seems a good approximation of the observed cosmography and agrees very well with the Λ CDM model so that we can argue that GRBs could be good distance indicators at redshift values up to $z = 4$.

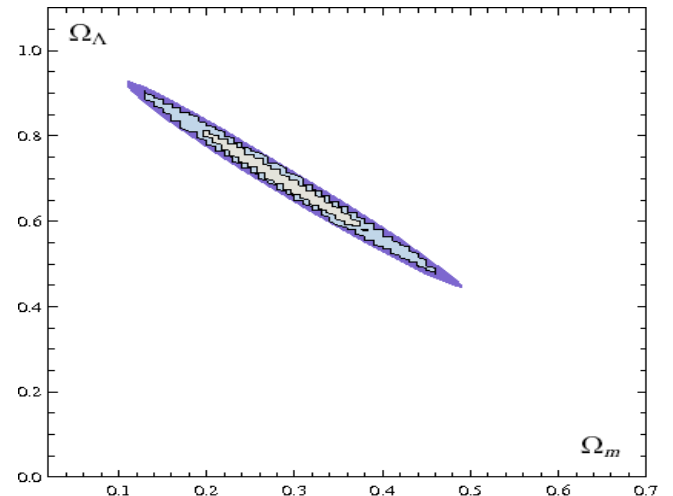


Fig. 8. 68%, 95% and 98% constraints on Ω_m and Ω_Λ , see Fig.(8) obtained from UNION sample and the GRB sample corrected for the 3 wrong GRBs.

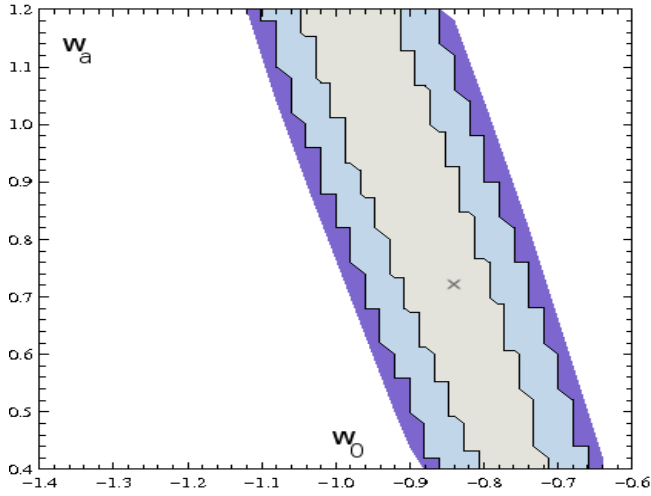


Fig. 9. 68%, 95% and 98% constraints on w_0 and w_a obtained from UNION sample and the GRB sample corrected for the 3 wrong GRBs. The cross represents the best fit value and it is in a good agreement with what found using the theoretical model described in Sect.2.

5. Discussion and Conclusions

Starting from the Friedmann equation, we have investigated a new method to constrain the cosmological Equation of State at high redshifts. The working hypothesis lies on the use of GRBs as distance indicators at high redshift, well beyond the distance where SNeIa are detected up to date. The CPL parameterization for the EoS has been explicitly used for the whole matter-energy content of the Universe as a suitable approach to investigate the parameter $w = w(z)$ and discriminate with respect to the Λ CDM model. In particular, regarding the Friedmann equations, for which

$$\frac{H'}{H} = \frac{(1+q)}{(1+z)}, \quad (19)$$

where q is the deceleration parameter and where the prime denotes the derivative with respect to the redshift, we have obtained, in the case of the LZ relation, with a reliable confidence level, the epoch for the transition between the deceleration-acceleration phases at a redshift value of $z \approx 5$. This is a value that, also if higher than the redshift of the farther GRB used, could be in agreement with current quasar formation scenarios. Besides, we are in good agreement with the observed phantom/quintessence regime at present epoch, that is for $z \rightarrow 0$, we obtain $w \leq -1$. However we have found an anomaly at $z \approx 4$ and beyond for which we rejected 3 GRBs at that distances. Several explanations are possible for this problem which can be summarized as:

- the effective cosmology is not described by the Λ CDM model
- the GRBs evolve with the redshift
- there is some nuclear or electromagnetic processes between the γ photons and the baryons involved in a GRB that would dim the observed flux or fluence.

Table 4. Results of the fits corrected for the 3 “wrong” GRBs. SNeIa is just for the Supernova Ia data, LZ is for the GRBs data obtained from the Liang-Zhang relation, GGL for the Ghirlanda et al. one.

Relation	w_0	w_a	R^2
LZ + SNeIa	-0.95 ± 0.01	0.74 ± 0.01	0.999
GGL + SNeIa	-0.865 ± 0.005	0.66 ± 0.005	0.999

Nevertheless such issues still remain unsolved and it represents a challenge. With this fact in mind, we have performed the same analysis without these 3 GRBs obtaining different results from the previous ones. In particular, we rejected the today phantom regime by this new analysis, obtaining for w_0 a value in agreement with the Λ CDM model at present epoch. The method, also if preliminary, seems to indicate that GRBs could be actually used as standard candles once a reliable unified model for the photometric and spectroscopic quantities is achieved (reliable results in this sense are presented in (Ghisellini et al 2008)). However, more robust samples of data are needed and more realistic EoS (with respect to the simple perfect fluid models) should be taken into account in order to suitably track redshift at any epoch (see for example (Capozziello et al. 2006)).

With the improving of the observations, in particular with the launch of new satellites devoted to the GRB surveys, as Fermi-GLAST³ and AGILE⁴, one should be able to expand the samples of GRBs, possibly with data coming from objects at higher redshift.

In summary, considering these preliminary results, it seems that GRBs could be considered as a useful tool to remove degeneration and constrain self-consistent cosmological models. Furthermore the matching with other distance indicators would improve the consistency of the Hubble distance-redshift diagram by extending it up to redshift 6 – 7 and over.

We wish to thank Riccardo Benini for useful discussions and suggestions.

References

- Albrecht, A., et al, 2006, arXiv:astro-ph/0609591
 Barboza Jr, E.M., & Alcaniz, J.S., 2008, Phys Lett B, 666, 415
 Basilakos, S., & Perivolaropoulos, L., 2008, MNRAS, 391, 411
 Bjornsson, G., et al. 2001, ApJ, 552, L121
 Branch, D., & Tammann, G. A., 1992, Ann. Rev. Astron. Astrophys., 30, 359
 Capozziello, S., V.F. Cardone, V.F., Elizalde, E., Nojiri, S., Odintsov, S.D., 2006, Phys. Rev. D **73**, 043512
 Capozziello, S., & Izzo, L., 2008, A&A, 490, 31
 Capozziello, S., Cardone, V.F., Salzano, V. 2008, Phys. Rev. D **78**, 063504.
 Chevallier, M., Polarski, D., 2001, Int. J. Mod. Phys. D., 10, 213; Linder, E. V., 2003, Phys. Rev. Lett., **90** 091301
 Copeland, E.J., Sami, M., Tsujikawa, S., 2006, Int. J. Mod. Phys. D., **15**, 1753.
 Dainotti, M.G., Cardone, V.F., Capozziello, S., 2008, MNRAS, 391, L79
 De Lucia, G., et al., 2007, MNRAS, 374, 809
 Djorgovski, S. G., Kulkarni, S. R., Bloom, J. S., Frail, D., Chaffee, F., & Goodrich, R. 1999b, GCN Circ. 189, <http://gcn.gsfc.nasa.gov/gcn/gcn3/189.gcn3>
 Draper, N.R. & Smith, H., 1998, *Applied Regression Analysis* (Wiley, New York).
 Ellis, R., 1999, Phys. World, 6, 19
 Friedman, A. S., & Bloom, J. S., 2005, ApJ, 627, 1
 Ghirlanda, G., Ghisellini, G., & Lazzati, D., 2004, ApJ, 616, 331
 Ghirlanda, G., Ghisellini, G., & Firmani, C., 2006, New Journal of Physics, 8, 123
 Ghisellini, G., et al., 2008, arXiv: 0811.1038 [astro - ph]

³ <http://fermi.gsfc.nasa.gov>

⁴ <http://agile.rm.iasf.cnr.it>

Table 3. Cosmological density parameters, with uncertainties computed at 1σ confidence limit, obtained from the MC-like procedure

Sample	Ω_m	Ω_Λ	Ω_k	χ^2
UNION + GRB	0.26 ± 0.14	0.73 ± 0.14	0.01 ± 0.04	1.032
UNION + GRB corrected	0.25 ± 0.10	0.74 ± 0.135	0.01 ± 0.035	1.00027

Table 5. GRBs Data Sample

GRB (1)	z (2)	E_p (keV) (3)	S_{bolo} (erg cm^{-2}) (4)	t_{jet} (days) (5)	θ_{jet} (deg.) (6)	n_0 (cm^{-3}) (7)
970508	0.84	389 ± 40	$8.09E-6 \pm 8.1E-7$	25 ± 5	23 ± 3	3.0 ± 2.4
970828	0.96	298 ± 30	$1.23E-4 \pm 1.2E-5$	2.2 ± 0.4	5.91 ± 0.79	3.0 ± 2.4
980703	0.97	254 ± 25	$2.83E-5 \pm 2.9E-6$	3.4 ± 0.5	11.02 ± 0.8	28.0 ± 10
990123	1.61	604 ± 60	$3.11E-4 \pm 3.1E-5$	2.04 ± 0.46	3.98 ± 0.57	3.0 ± 2.4
990510	1.62	126 ± 10	$2.85E-5 \pm 2.9E-6$	1.6 ± 0.2	3.74 ± 0.28	0.29 ± 0.14
990705	0.84	189 ± 15	$1.34E-4 \pm 1.5E-5$	1 ± 0.2	4.78 ± 0.66	3.0 ± 2.4
990712	0.43	65 ± 10	$1.19E-5 \pm 6.2E-7$	1.6 ± 0.2	9.47 ± 1.2	3.0 ± 2.4
991216	1.02	318 ± 30	$2.48E-4 \pm 2.5E-5$	1.2 ± 0.4	4.44 ± 0.7	4.7 ± 2.8
010222	1.48	309 ± 12	$2.45E-4 \pm 9.1E-6$	0.93 ± 0.1	3.03 ± 0.14	3.0 ± 2.4
011211	2.14	59 ± 8	$9.20E-6 \pm 9.5E-7$	1.56 ± 0.16	5.38 ± 0.66	3.0 ± 2.4
020124	3.20	87 ± 18	$1.14E-5 \pm 1.1E-6$	3 ± 0.4	5.07 ± 0.64	3.0 ± 2.4
020405	0.70	364 ± 90	$1.10E-4 \pm 2.1E-6$	1.67 ± 0.52	6.27 ± 1.03	3.0 ± 2.4
020813	1.25	142 ± 14	$1.59E-4 \pm 2.9E-6$	0.43 ± 0.06	2.8 ± 0.36	3.0 ± 2.4
021004	2.32	80 ± 53	$3.61E-6 \pm 8.6E-7$	4.74 ± 0.5	8.47 ± 1.06	30.0 ± 27.0
030226	1.98	97 ± 27	$8.33E-6 \pm 9.8E-7$	1.04 ± 0.12	4.71 ± 0.58	3.0 ± 2.4
030328	1.52	126 ± 14	$6.14E-5 \pm 2.4E-6$	0.8 ± 0.1	3.58 ± 0.45	3.0 ± 2.4
030329	0.17	67.9 ± 2.3	$2.31E-4 \pm 2.0E-6$	0.5 ± 0.1	5.69 ± 0.5	1.0 ± 0.11
030429	2.66	35 ± 12	$1.13E-6 \pm 1.9E-7$	1.77 ± 1.0	6.3 ± 1.52	3.0 ± 2.4
041006	0.71	63 ± 12	$1.75E-5 \pm 1.8E-6$	0.16 ± 0.04	2.79 ± 0.41	3.0 ± 2.4
050318	1.44	47 ± 15	$3.46E-6 \pm 3.5E-7$	0.21 ± 0.07	3.65 ± 0.5	3.0 ± 2.4
050505	4.27	70 ± 23	$6.20E-6 \pm 8.5E-7$	0.21 ± 0.04	3.0 ± 0.8	3.0 ± 2.4
050525	0.61	81.2 ± 1.4	$2.59E-5 \pm 1.3E-6$	0.28 ± 0.12	4.04 ± 0.8	3.0 ± 2.4
050904	6.29	436 ± 200	$2.0E-5 \pm 2E-6$	2.6 ± 1	8 ± 1	3.0 ± 2.4
051022	0.80	510 ± 22	$3.40E-4 \pm 1.2E-5$	2.9 ± 0.2	4.4 ± 0.1	3.0 ± 2.4
060124	2.30	237 ± 76	$3.37E-5 \pm 3.4E-6$	$1.2 \pm$	3.72 ± 0.15	3.0 ± 2.4
060210	3.91	149 ± 35	$1.94E-5 \pm 1.2E-6$	0.33 ± 0.08	1.9 ± 0.17	3.0 ± 2.4
060526	3.21	25 ± 5	$1.17E-6 \pm 1.7E-7$	1.27 ± 0.35	4.7 ± 1	3.0 ± 2.4

References: (Jimenez et al. 2001); (Metzger et al. 1997); (Djorgovski et al. 1999); (Kulkarni et al. 1999); (Israel et al. 1999); (Bjornsson et al. 2001); (Li et al.)

Israel, G., et al. 1999, A&A, 348, L5
Jimenez, R., Band, D., & Piran, T., 2001, ApJ, 561, 171
Kelner, S. R., 2008, Phys. Rev. D, 78, 034013
Komatsu, E., et al, 2008, arXiv: astro-ph/0803.0547
Kowalski, M., et al, 2008, ApJ, 686, 749
Kulkarni, S. R. et al., 1999, Nature, 398, 389
Li H. et al., 2008, Apj, 680, 92
Liang, N., et al, 2008, ApJ, 685, 354
Liang, E., & Zhang, B., 2005, ApJ, 633, 611
Meszaros, P., 2006, Rept. Prog. Phys., **69** 2259
Metzger, M. R., Djorgovski, S. G., Kulkarni, S. R., Steidel, C. C., Adelberger, K. L., Frail, D. A., Costa, E., & Frontera, F. 1997, Nature, 387, 878
Perivolariopoulos, L., & Shafieloo, A., 2008, arXiv: 0811.2802
Razzaque, S., et al., 2009, arXiv: 0901.4973
Riess, A. G., et al., 1998, ApJ, 116, 1009
Romeo, A. D., et al., 2008, MNRAS, 389, 13
Rowan-Robinson, M., 1985, *The Cosmological Distance Scale* (Freeman & co., New York)
Ruffini, R., et al, 2008, *Gamma Ray Bursts. Proceedings XI Marcel Grossmann Meeting*, (World Scientific, Singapore)
Sari, R., Piran, T., & Halpern, J. P., 1999, ApJ, 519, L17
Schaefer, B. E., 2007, ApJ, 660, 16
Stott, J. P., et al., 2009, MNRAS 2009, MNRAS, 394., 2098S
Visser, M., 2004, Class. Quant. Grav., **21**, 2603
Visser, M., & Cattoën, C., 2007b, arXiv: gr-qc/0703122
Weinberg, S., 1972, *Gravitation and Cosmology: Principles and applications of the general theory of relativity*, (Wiley, New York)
Zdziarski, A. A., and Svensson, R., 1989, ApJ, 344, 551